Acta Materialia 255 (2023) 119081

Contents lists available at ScienceDirect

Acta Materialia

journal homepage: www.elsevier.com/locate/actamat

Role of Ag segregation on microscale strengthening and slip transmission in an asymmetric Σ5 copper grain boundary

Mohammed Kamran Bhat, Prithiv Thoudden Sukumar, Lena Langenohl, James P. Best *, Gerhard Dehm *

Max-Planck-Institut für Eisenforschung GmbH, 40237 Düsseldorf, Germany

ARTICLE INFO

Keywords:
Micropillar compression
Dislocation transmission
Grain boundary segregation
Strength

ABSTRACT

Micropillar compression was used to investigate whether Ag segregation to an asymmetric Σ5[001] grain boundary will lead to measurable strength differences compared to the pure copper bicrystal. Ag segregation was accomplished by deposition and subsequent annealing of an Ag thin-film applied on the surface of the Cu bicrystal. Atom probe tomography analysis indicated Ag segregation at the grain boundary with a peak concentration of 2.3 at.%. While the pristine Σ5 grain boundary shows a yield strength of 288 ± 18 MPa when compressing 1 μm diameter pillars along ⟨001⟩, micropillars containing an Ag-segregated Σ5 grain boundary demonstrated an increased yield strength of 318 ± 17 MPa. In addition, post-deformation electron microscopy was carried out to examine the active slip systems and slip transmission across Ag-free and Ag-containing bicrystals. The results are compared to reference measurements of the adjacent single crystal grains. The 1 μm pillar diameter promoted deformation governed by dislocation-grain boundary interactions for the bicrystalline pillars. This is the first time that changes in flow stress associated with grain boundary segregation have been quantified locally without interference from other mechanisms such as solid solution strengthening, formation of precipitates or changes in stacking fault energy. The results clearly indicate that purely geometrical models for slip transmission are not sufficient as the local atomic structure and composition influence dislocation transmission through grain boundaries.

1. Introduction

The study of grain boundaries (GBs) is of critical importance and there are few systematic investigations that directly correlate GB structure and chemistry to physical properties [1–3]. Mechanical behaviour is one key property influenced by GBs, where dislocation-GB interactions play an important role [3–6]. Studies of slip interactions at GBs started roughly 60 years ago, with Livingston and Chalmers analysing slip transfer across GBs in bicrystals [7]. In general, dislocation-GB interactions may have the following outcomes: (i) direct transmission; (ii) direct transmission with a residual Burger's vector left at the GB; (iii) indirect transmission assisted by non-conservative movement across the GB (e.g. through dislocation climb); (iv) no transmission, which could be due to complete absorption of the incoming dislocation or the GB acting as a strong barrier to dislocation transmission; (v) the GB acts as dislocation source [8]. For a more detailed description on dislocation-GB interactions, readers are directed to the review articles of Refs. [9–11]. An approach to parametrise the likelihood of slip transfer between grains was taken by Luster and Morris [12], who defined the transmission factor $m' = \cos\Psi \cdot \cos\kappa$ as a geometric function of the angles between slip plane normals in each grain (Ψ) and the slip vectors (κ), with slip transmission occurring when m' is close to unity (perfect transmission), but blocked when m' approaches zero. Experimentally determining m' is straightforward based on electron backscatter diffraction (EBSD) data. Furthermore, based on both molecular dynamics (MD) simulations and experiments, m' is found to consistently predict the likelihood of slip transmission [10,13-15].

Micro- and nanomechanical methods have been employed to study the influence of GBs and slip transmission in both FCC and BCC metals [13,16-20,21-24]. Over the last two decades, micropillar compression has demonstrated its importance for understanding GB-dislocation interactions, with research groups examining the mechanical response of isolated GBs in pure FCC and BCC metals using this technique [13,16,17,19–22]. While nanoindentation provides fast, precise local mechanical

* Corresponding authors.
E-mail addresses: j.best@mpie.de (J.P. Best), g.dehm@mpie.de (G. Dehm).

https://doi.org/10.1016/j.actamat.2023.119081
Received 30 January 2023; Received in revised form 16 May 2023; Accepted 8 June 2023
Available online 10 June 2023
1359-6454/© 2023 The Authors. Published by Elsevier Ltd on behalf of Acta Materialia Inc. This is an open access article under the CC BY-NC-ND license (http://creativecommons.org/licenses/by-nc-nd/4.0/).

characterisation with minimal surface preparation, micropillar compression offers a clearer observation and analysis of activated/-transmitted slip steps in addition to extracting load-displacement data under a nominally uniaxial stress state [25]. A major disadvantage of pillar compression is that at sub-micron length-scales a highly stochastic response is prevalent [26]. However, testing bicrystals at such length scales also allows for the load-displacement data to be dominated by dislocation-GB interactions [17,27]. Although *in situ* transmission electron microscopy (TEM) facilitates the observation of dislocation-GB interactions at the atomic scale, it is well known that thin TEM foils have extremely high stresses due to sample size effects [28], which impede quantitative interpretation. For more detailed overview on the emergence and advancements in micro- and nanomechanical testing readers are directed to Ref. [29].

MD studies at high strain rates of typically 10^8 s^{-1} have linked the transmission stress across a GB to the GB energy (usually referred to as energy criterion) [14,30], revealing an increase in the energy barrier for slip transmission with decreasing GB energy. Adlakha *et al.* found this correlation in pure α-Fe but also for hydrogen enriched GBs in α-Fe [30]. Huang *et al.* demonstrated a correlation between the change in the excess free volume as a function of impurity segregation for a Σ5[310] GB in Cu, and strengthening, using first-principle calculations [31]. In their study, the decrease in GB energy was attributed to the efficiency of impurities or dopants in filling the excess free volume at the GB, and the strengthening effects were found to be closely related to the electronic interactions between the segregating elements and host Cu atoms. Currently, there are few experimental proofs for the energy criterion [32,33], and although the above discussed geometric parameter *m*' addresses the crystallographic dependence of slip transmission across a GB, surprisingly there exist a limited number of systematic experimental attempts to comprehensively understand the influence of other parameters such as temperature, strain rate or local chemistry on dislocation-GB interactions. These interactions are of paramount importance in predicting and controlling deformation and failure at these interfaces. In their pioneering attempt, Malyar *et al.* [34] addressed the impact of varying strain rates on the dislocation transmission by testing bicrystalline copper micropillars containing a penetrable high-angle GB at strain rates of 10^{-4} to 10^{-1} s^{-1}. The measurements revealed a clear strain rate sensitivity (SRS) of the bicrystalline pillars, four times higher than for their single-crystalline counterparts. The difference in the SRS was attributed to the difficulty in reorienting dislocations in adjacent grains at higher strain rate and the non-conservative motion of dislocations in the GB plane (thermally activated process) was speculated to be most likely the origin of the quantitative differences in SRS of the single and the bicrystalline micropillars. Furthermore, the SRS of bicrystalline micropillars approaches single crystalline micropillars at higher strains, as indirect slip transmission becomes prevalent.

For nanocrystalline metals/alloys the maximum strength corresponds to competing dislocation and GB-mediated mechanisms [35]. The current understanding of how individual deformation mechanisms contribute to the overall deformation behaviour of polycrystalline/nanocrystalline materials is limited and there is a significant gap in the quantitative understanding of individual mechanisms [36]. While GB segregation offers a viable approach in manipulating GBs to tailor the "strongest grain size" and mechanical properties [24,32,35,37-39], the influences of GB chemistry on slip transmission, an essential part of both dislocation and GB mediated deformation mechanisms has not yet been systematically investigated [10]. Although experiments on bulk-polycrystalline specimens provide valuable information, they provide rather indirect global evidence [32,33]. In polycrystals this is due to deformation activity in surrounding grains leading to complex local stress states and activation of different slip systems, while the inherent microstructural complexities such as precipitate formation in multi-element systems and variations in impurity segregation across different boundary types further complicates analysis [40–42].

Here, by employing *in situ* scanning electron microscope (SEM) micropillar compression with support from slip trace analysis and atom probe tomography measurements for chemical analysis, this study attempts to systematically determine the influencing factor of solute segregation on slip transmission and mechanical response. The present study utilises a bulk Cu bicrystal containing an asymmetric Σ5<100> GB and Ag as segregating species. Cu-Ag is an immiscible system where Ag preferentially segregates to GBs [43], and acts as model system to experimentally investigate the change in slip transmission and flow stress associated with changing GB chemistry.

2. Experimental methods

2.1. Sample fabrication and characterisation

As described in Ref. [44], two seed crystals were employed to grow a bulk bicrystal from 99.97 at.% purity copper (See Supplementary Information **Table S1**) using the Bridgman method. Subsequently, electro-discharge machining was performed to cut out two 0.4 mm thin bicrystalline slices from the mother bicrystal. The slices were further ground and electropolished using phosphoric acid at a voltage of 22 V ensuring a clean and a damage-free surface. One of the slices was sputter coated with a 500 nm Ag layer (Bxx(Ag)), while as a reference the other slice was left in a pristine state (Bxx). Both of these slices were annealed at 800 °C (1073 K) for 120 h under a protective Ar atmosphere. Post-annealing, the specimen surfaces were Argon ion polished using a broad ion beam (Gatan PECS II). Bicrystal slices were characterised by electron backscatter diffraction (EBSD) in a Zeiss Auriga® dual-beam focused ion beam (FIB)–SEM with an attached EDAX TSL-OIM version 6.0 data acquisition system.

2.2. Scanning transmission electron microscopy

Conventional TEM preparation was used to estimate the initial dislocation content in the grains. Initially, the sample was mechanically thinned to 200 μm. Then, the samples were electropolished using a TenuPol-5 in 33% HNO_3 in Methanol at 2 V and a temperature of −30 °C. For extracting site-specific TEM lamellae at the Ag-segregated GB, a Thermo Fisher Scientific Scios2HiVac dual-beam SEM was used. The rough milling was performed at 30 kV and 1 nA, going sequentially down to 5 kV and 7.7 pA up to a thickness of about 80 nm. A FEI Titan Themis 80–300 (Thermo Fisher Scientific) scanning TEM (STEM) was used for imaging. The DF-STEM dataset was taken with collection angles of 25 to 154 mrad, whereas the TEM image was taken with a 4k Ceta camera from FEI.

2.3. Probing GB segregation

A correlative approach consisting of EBSD, transmission Kikuchi diffraction (TKD), and site-specific atom probe tomography (APT) was utilised to analyse the GB. APT tips were prepared using a dual-beam FEI Helios NanoLab 660i FIB–SEM. TKD was performed with an EDAX Hikari Plus EBSD camera during the FIB preparation to ensure the presence of the targeted GB. A standard lift-out procedure was employed for APT tip preparation. APT studies were carried out in a LEAP 5076XS and the measurement was carried out at 50 K with a detection rate of 0.7% (7 ions per 1000 pluses). Laser pulsing with a repetition rate of 200 kHz and pulse energy of 60 pJ was used. Cameca's AP suite 6.1 software was employed for analysing the acquired data. The interfacial excess of Ag from the APT measurement was calculated using the integral method as described in Ref. [45].

2.4. Micropillar fabrication, testing and post-deformation analysis

Both single (Sxx) and bicrystalline (Bxx) cylindrical micropillars with a top diameter of ~1 μm were fabricated by Ga^+ FIB milling at 30 kV

with currents of 2 nA down to 240 pA for final polishing (Zeiss Auriga® dual-beam FIB-SEM). Nano Patterning and Visualization Engine (NPVE) software was employed for annular milling leading to a typical cylindrical pillar as seen in Fig. 1**a**. For each prepared pillar, dimensions were first determined using SEM imaging. The GB was parallel to the loading direction and extended throughout the bicrystalline pillars. A diameter-to-height aspect ratio of 1:2.5–3.0 was maintained. This configuration facilitates dislocation-GB interaction as described in Ref. [46,47]. The *in situ* micropillar compression tests were carried out using a Bruker Hysitron PI 88 mounted in a Zeiss Gemini 500 SEM. The indenter tip was a conductive diamond flat punch with 3 μm diameter (Synton-MDP, Switzerland). All tests were performed in pseudo-displacement-controlled mode at a strain rate of 10^{-3} s^{-1}. The yield stress (σ_y) was defined as the maximum stress at or prior to 2% offset strain (for a more detailed description see Supplementary Information). The majority of the tests were conducted to engineering strains greater than 10% to obtain well-defined slip steps (see Supplementary Information **Fig. S8**). The cross-sectional diameters at the top of each pillar were taken as the representative diameter to calculate the engineering stress values [48]. A total of 32 micropillars were successfully tested. Compression tests were followed by post-mortem SEM imaging, to assist in verifying glide step crystallography. A Mathematica© code was used to visualise and simulate the slip traces of single-crystalline counterparts and slip transmission factors (m') for relevant slip systems were calculated using the STABIX tool [49].

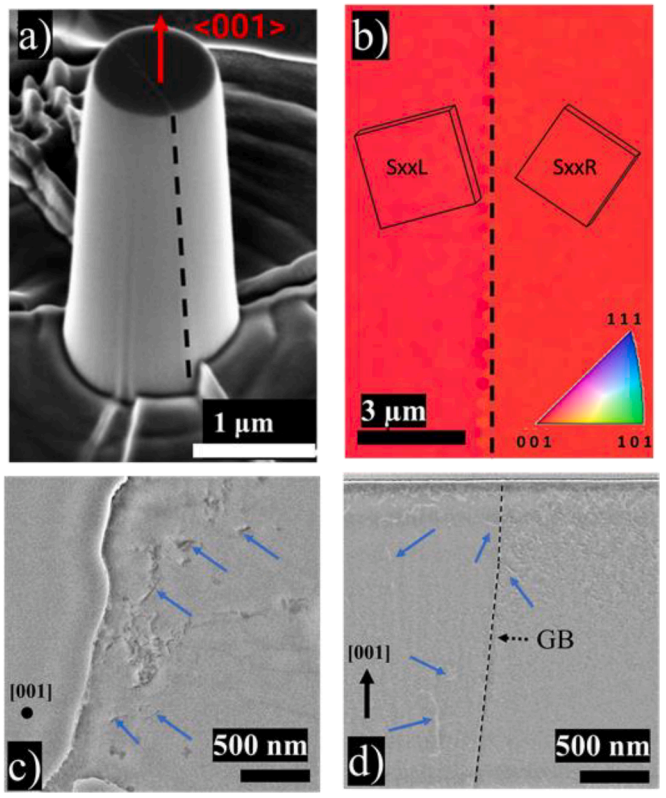

Fig. 1. a) A representative bicrystal pillar (Bxx) before compression (GB highlighted with dashed black line); b) EBSD inverse pole-figure (IPF) map of the bicrystal showing the GB trace (dashed black line) and relative crystal orientations in ⟨001⟩ zone axis. c) BF-TEM micrograph of conventionally prepared foil of the Ag-free specimen used to estimate dislocation density. The distribution is heterogenous, showing μm^2 areas free of dislocations separated by areas containing entangled dislocations. Some dislocations are highlighted by blue arrows. d) DF-STEM image of a FIB lamella of the Ag segregated GB in cross-section, in which the left grain is in ⟨120⟩ zone axis. The distribution of dislocations is comparable to the Ag-free specimen. Some dislocations in c) and d) are highlighted by blue arrows.

3. Results and interpretation

3.1. GB segregation and mechanical response

The annealed bicrystal was found to contain a single asymmetric Σ5 [001] $(5\bar{1}0)/(210)$ tilt GB with a misorientation angle of 40 ± 1.6°, and surface normals (equivalent to the compression direction) ≈ ⟨001⟩ for grain pairs *L* [2 1 23] and *R* [2 1 27] (left *L* and right *R*, respectively, according to Fig. 1**b**). The GB planes $(5\bar{1}0)/(210)$ were determined using a stereographic projection from the EBSD data, where the indices correspond to the crystallographic planes of the abutting grains parallel to the GB plane (Fig. 1**b**). A representative cylindrical bicrystalline micropillar (Bxx) with 3° taper is illustrated in Fig. 1**a**, in which the GB is positioned close to the centre and extends across the pillar volume. The initial (post-annealing) dislocation density estimated using TEM of electrolytically thinned specimens (Bxx) was (9.5 ± 2.0) × 10^{12} m^{-2} (see Fig. 1**c** and **Fig. S9**). The dislocations are heterogeneously distributed, with dislocations free regions and areas containing dislocation entanglements. Of critical importance, site-specific TEM analysis of the Ag-segregated GB Bxx(Ag) revealed no significant secondary dislocation structures in the bulk or near the GB (see Fig. 1**d** and **Fig. S10**).

To determine the chemical compositions at the GB for the annealed diffusion couple, an APT specimen extracted close to the sample surface of Bxx(Ag) (Tip 1, Fig. 2**a**) was found to have a peak concentration of 2.3 at.% Ag (line composition indicated by the black arrow) at the GB (Fig. 2**c**). An APT specimen extracted approximately 2 μm below the surface (Tip 2, Fig. 2**b,d**) showed a GB concentration close to 1.4 at.% Ag, suggesting a concentration gradient of Ag along the specimen depth. As a consequence of the Ag segregation, and consistent with Ref. [44], the GB in Bxx(Ag) is observed to have inclinations varying between

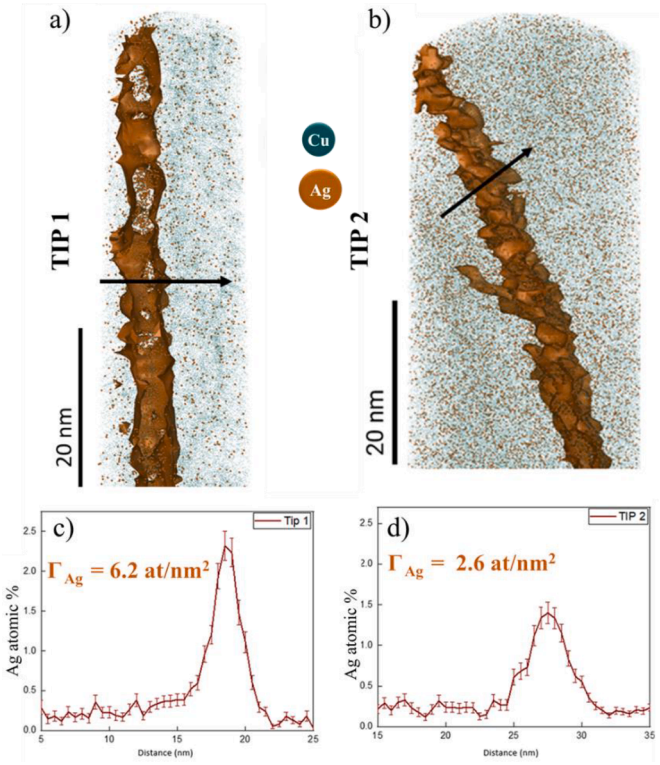

Fig. 2. (a-b) 3D reconstructed APT tip 1, extracted close to the top surface showing the Cu and Ag atoms and 0.8 at.% Ag isosurface at the GB. Tip 2 was extracted at an approximate depth of ~2 μm. Note that the grain boundary inclination in b) is predominately caused by extracting an inclined FIB-APT sample. (c-d) 1D concentration profiles (indicated by black arrows in a and b) corresponding to tip 1 and tip 2 show a peak concentration of 2.3 and 1.4 at.% Ag, respectively, at the GB. The values of Γ_{Ag} correspond to the GB excess.

0 and 9° (**Fig. S7**) rather than straight boundaries as for the Ag-free Bxx pillars (Fig. 1**a**). However, as reported in Ref. [47], inclinations of such magnitude have a negligible influence on the observed mechanical response and does not interfere in the final interpretation. Using the integral method [45], a solute excess of 6.2 ± 1.0 atoms/nm^2 was calculated for Tip 1 and 2.6 ± 0.5 atoms/nm^2 for Tip 2 at the GB, respectively. The same approach yields a matrix concentration of 0.18 at.% Ag, which can be rationalised when considering a room temperature solid matrix solubility of ~0.1 at.% according to the Cu-Ag phase diagram [43].

FIB-milled micropillars with ~1 μm diameter were then cut for pure and Ag segregated specimens. Compression testing of both the Sxx and Bxx micropillars revealed serrated stress-strain curves (Fig. 3), characteristic of stochastic deformation at micron length-scales [26]. As the deformation axis corresponds to [001] in both grains, eight {111} slip systems could be activated according to Schmid's law in each grain. Although dislocation-dislocation interactions could potentially mask the effect of dislocation-GB interactions, a clear impact of the asymmetric Σ5[001] (5$\bar{1}$0)/(210) tilt GB is observed when comparing the flow stress of the Bxx to that of the Sxx micropillars (Fig. 3**a**). The pristine Σ5 Bxx demonstrates a higher strength than its SxxL and SxxR single-crystalline counterparts. The higher strength in Bxx is explained by dominant dislocation–grain boundary interactions over dislocation-dislocation interactions. This can be attributed to the small pillar diameter of ~1 μm and the low initial dislocation density, as at these length scales, dislocations are also more likely to escape to the specimen surface minimising the probability for dislocation-dislocation interactions [17,27,29,50]. Thus, the deformation behaviour in the bicrystal pillars at this length-scale appears to be dominated by dislocation-GB interactions [51].

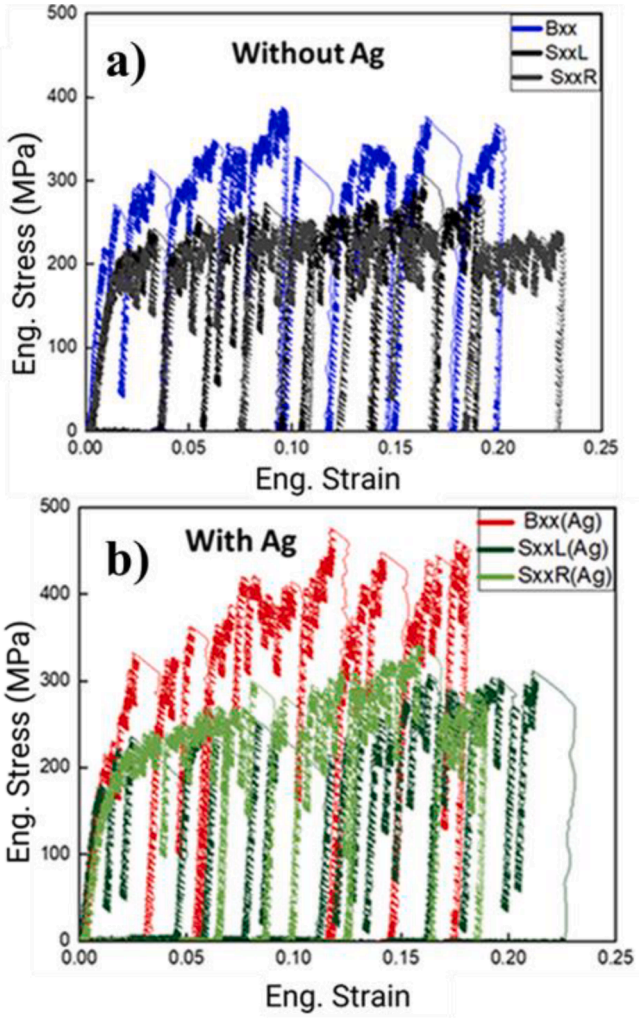

Fig. 3. Representative flow curves for a) the Cu reference specimen, and b) the Ag segregated specimen from micropillar compression. Responses from both single crystalline pillars and bicrystal are shown.

Flow curves for the Ag segregated specimens reveal a similar trend (Fig. 3**b**). The Bxx(Ag) micropillar shows significantly higher strength than the constituent SxxL(Ag) and SxxR(Ag) responses, exceeding the flow stresses obtained for the pristine Bxx sample(s). This trend is further established when the yield strength (σ_y) is compared for all tested specimens (Fig. 4). Single crystalline micropillars of the pristine and Ag containing specimens show similar flow stress responses (Fig.4**a, c**). However, with Ag segregation the strength of the Bxx(Ag) samples yield at 318 ± 17 MPa, while the Ag-free Bxx reaches yield stresses of 288 ± 18 MPa.

3.2. Slip trace analysis

3.2.1. Single-crystalline micropillars

Fig. 5**a-d** show representative post-deformation SEM images and simulated slip traces of the single crystalline pillars Sxx(Ag). Multiple fine and a few large slip steps were observed in the single crystalline samples SxxL(Ag) and SxxR(Ag), and are consistent with the simulated slip traces with the highest Schmid factors. No differences are found between Sxx pillars both without and with 0.18 at.% Ag. The total number of possible active slip systems are summarised in **Table S2**, in decreasing order of Schmid factor. Three distinct slip systems could be identified in both the left and the right single-crystalline micropillars respectively. The slip traces corresponding to the highest Schmid factor slip systems are identified in Fig. 5**a-d**.

3.2.2. Bicrystalline micropillars

Upon examining the post-deformation surface features of the bicrystals by SEM, the deformed pillars show multiple small slip steps in both grains originating from multiple active slip systems (Fig. 6). Examining the slip traces, several slip lines are seen to extend from one grain through the GB to the abutting grain, evidence of possible slip transmission through the GB. The slip traces of Fig. 6 correspond to the slip systems shown in Fig. 5 of 1 L (red) and 2R (blue) with Schmid factors of 0.422 and 0.418 for grain L and grain R, respectively, and a calculated transmission factor m' = 0.63, indicating a favourable transmission configuration. While there exist multiple combinations of active slip systems with even higher transmission factors (see **Table S3**), due to the continuity of slip across the GB (as highlighted by the white dashed arrows in Fig. 6) and dominant slip traces, the aforementioned combination was resolved, and the continuity of slip traces across the GB strongly serves as an indicator of direct dislocation transmission [52].

Testing a boundary with Ag decoration makes it possible to gain more insights into dislocation-GB interactions using local chemical tomography analysis. Fig. 7 compares pre- and post-deformation 3D APT reconstructions, wherein the post-deformation APT tip was extracted from a Bxx(Ag) micropillar deformed to an engineering strain of 14%. While the pre-deformation APT specimen extracted from a region in close vicinity to the deformed pillar reveals a straight GB segment (Fig. 7**a**, consistent with Fig. 2), deformation is seen to induce significant steps into the GB (Fig. 7**b**). The observed steps (on the order of 10–15 nm width) are assumed to be a direct result of residual disconnections at the GB due to frequent dislocation GB interactions (see also Supplementary Video 1,2 and **Table S4**). It must be noted that despite the micropillar being deformed to 14% engineering strain, the GB steps in the post deformation APT should reflect a strain less than 14% due to the localised slip during the micropillar compression. Nevertheless, the post-deformation images and post-deformation APT combined with the transmission factors of the active slip systems suggest frequent dislocation-GB interactions (dislocation-transmission) within the

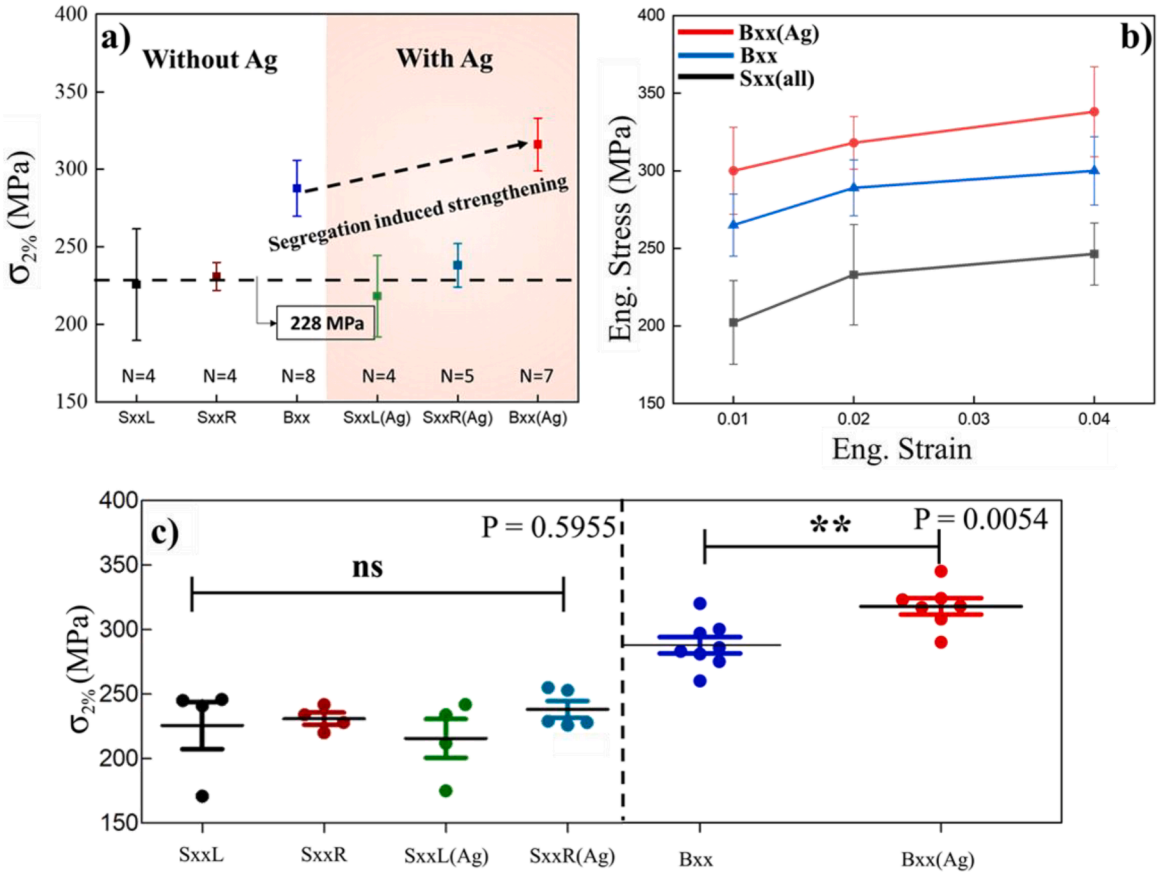

Fig. 4. a) Comparison of the average yield stress (σ_y) of specimens based on the number of samples (*N*) tested successfully. Error bars represent single standard deviations. The mean flow stress of 228 MPa for all single crystal samples Sxx and Sxx(Ag) is represented with a dashed black line. b) Comparison of flow stress values at 1%, 2% and 4% strain offset. Single crystalline pillars of both specimens are grouped into a single category Sxx(all). c) Unpaired Student's t-tests were performed on $\sigma_{2\%}$ for statistical significance (not-significant *ns* when $P > 0.05$, significant ** when $P \leq 0.01$). Error bars denote standard error of the mean.

deforming volume of the bicrystals. A more detailed discussion on the implications of these observations is provided in the next section.

4. Discussion

While the yield strength comparisons in Fig. 4 reveal a clear correlation between strength and GB chemistry for the bicrystal samples, the post-deformation images of slip traces (Fig. 6) show no obvious differences between the Bxx and Bxx(Ag) samples. Given that dislocation-GB interactions are predicted to dominate the deformation response, the differences in mechanical behaviour must arise through differences in the slip transmission. Potential factors that may affect the mechanical response/dislocation transmission across the GB include:

i. The relative orientation of slip systems across the GB;
ii. The formation and operation of dislocation sources in the bulk and/or near to the GB;
iii. Possible secondary dislocation structure near Ag-segregated GB;
iv. Ag enrichment at the GB;
v GB acts as dislocation source;

Factor (i) relating to the transmission factor *m*' is purely geometric where a high *m*' indicates easier slip continuity across the GB, thus favouring slip transmission. Structural and chemical effects of the GB are not considered. As a consequence, the post-deformation images (Fig. 6) clearly identify the same glide systems for Bxx(Ag) and the Ag free Bxx, and (i) can therefore be ruled out as a possible cause of strength increase.

The impurity content in the bulk/near GB may also result in increased resistance to dislocation motion (solid solution strengthening) further impairing the operation of dislocation sources and dislocation propagation i.e. factor (ii). However, in the present study, the atom probe results of Fig. 2 indicate an average concentration of only 0.18 at.% Ag in the bulk. For Cu with a moderate stacking fault energy (SFE) of 70 mJ•m^{-2} [53], the addition of 0.18 at.% Ag will have a negligible influence on the SFE [54]. Also, while the lower shear modulus and larger atomic size of Ag compared to Cu may lead to some solid solution strengthening, based on the Fleischer model 0.18 at.% Ag is predicted to only increase the shear strength by 1.7 MPa ($\approx$ 4.4 MPa in yield strength) [55] (Supplementary Information, Section S2). This is in accordance with the observed stress-strain responses revealing no impact on the single crystalline yield stress (Fig. 3) compared to the pristine reference specimen (see Fig. 4). Therefore, no evidence was found to attribute solid solution hardening or changes in SFE in the bulk as the possible causes of the strength enhancement, nor was Ag precipitation observed within the grains or at the grain boundaries. As earlier put forth in Section 3.1, no evidence of an existent secondary dislocation structure near the Ag-segregated GB was found hence (ii) and (iii) as putative factors influencing strength could be ruled out.

In light of the aforementioned results and discussions, explanations for the strength increase point towards factor (iv); i.e. that the change in mechanical behaviour (i.e. strengthening) could primarily be influenced by Ag enrichment at the GB. The addition of the relatively larger Ag atom along the GB could potentially induce local distortion. As dislocation-GB interactions are sensitive to local stress fields [56], dislocation movement may consequently be influenced, resulting in higher transmission stresses. The observations made here also align with MD observations made for the Cu-Zr system [57]. In that study [57], segregated Zr atoms lead to strong dislocation pinning at the GB by

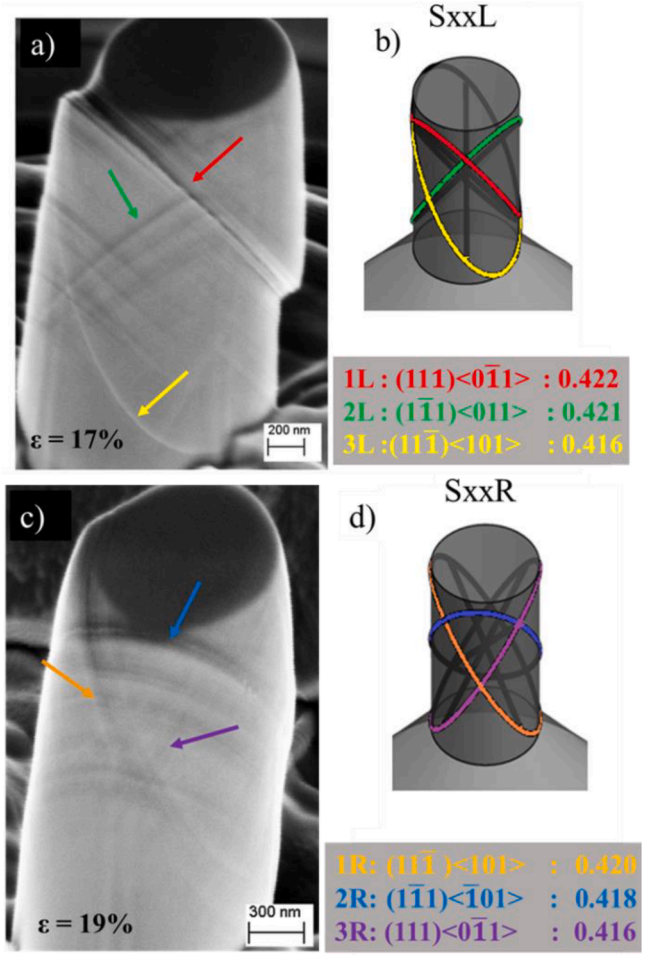

Fig. 5. a,c) Representative post-deformation SEM images of single-crystalline specimens Sxx(Ag). b,d) Corresponding simulated slip systems in single-crystalline micropillars with calculated Schmid factors, where the systems with the three highest Schmid factors are highlighted, and denoted in a,c) with arrows.

formation of ledges and local strain fluctuations, increasing the flow stress required for dislocation propagation. Interestingly, dislocation pinning by a GB was experimentally observed during *in situ* TEM compression of pure Cu Σ5 GB containing pillars [58], consistent with the performed MD simulations [57]. Furthermore, MD simulations on a symmetric Cu Σ5{210} GB with and without Ag reveal an increase in excess volume and change in GB shear stresses, both opposing transmission in case of Ag segregation [31,57]. Moreover, recent experimental evidence of strain rate sensitivity of pure Cu bicrystalline pillars during micropillar compression indicates stress-assisted non-conservative dislocation movement as an essential phenomenon during slip transmission [34]. Therefore, the segregation of Ag atoms at the GB would additionally reduce the GB diffusivity, limiting stress-assisted dislocation climb up or down along the GB plane eventually

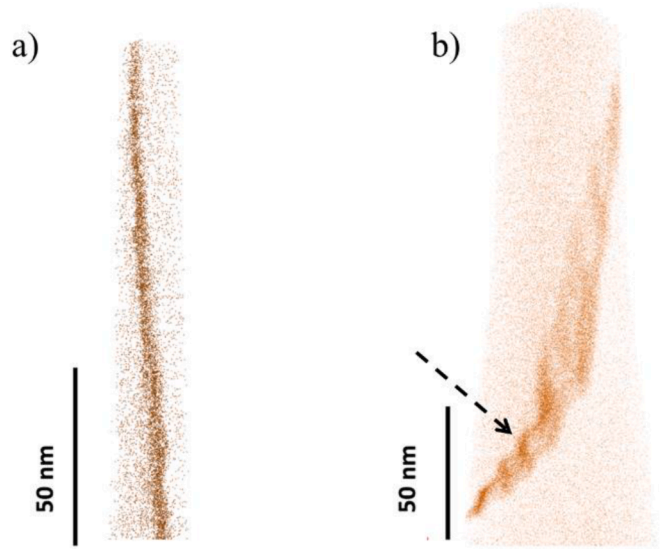

Fig. 7. a) 3D reconstructed APT tip showing only Ag atoms, and b) APT tip extracted from a deformed pillar with a total engineering strain of 14%. Post-deformation APT results indicate significant steps (highlighted by the black arrow) in the GB after undergoing deformation.

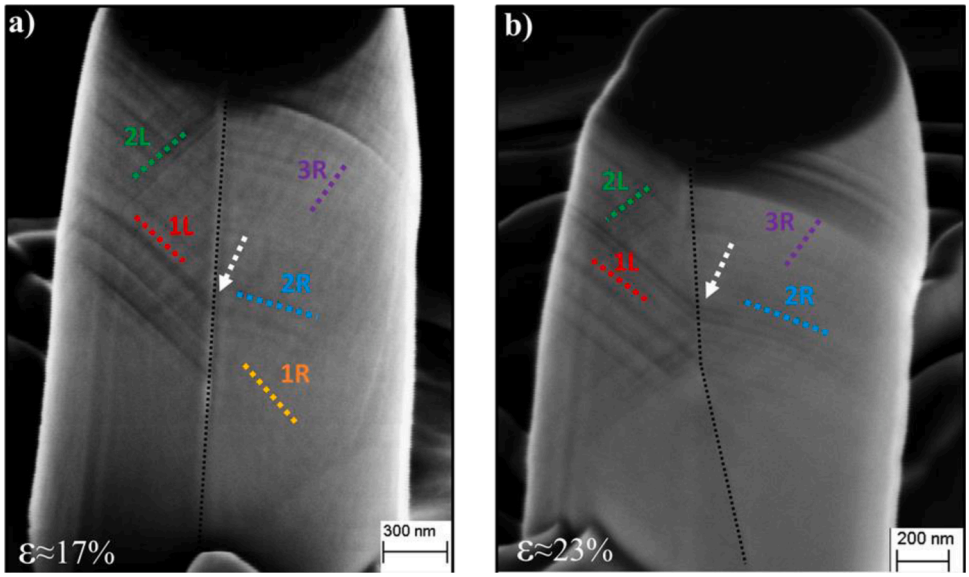

Fig. 6. Post-mortem SEM images of a) representative Bxx (compressed to ~17% strain) and b) Bxx(Ag) (compressed to ~23% strain), where the markings indicate slip traces on the left and right grain component. Attention is paid to the continuity of slip traces 1L and 2R across the GB (indicated by the white arrow) in both cases indicative of direct dislocation transmission.

restricting indirect slip transmission [59,60]. As such, based on the current experimental observation of higher shear stresses measured in the case of the Ag enriched GB, it is implied that the GB chemistry and local atomic-scale GB properties influence the transmission stress [15].

It follows that GB chemistry is an instrumental parameter in engineering the Hall-Petch coefficient k [61], as demonstrated in polycrystalline nickel doped with sulphur, where tensile tests indicated an increase in the Hall-Petch slope with sulphur concentration [62]. This was explained based on sulphur segregation increasing the ledge density at the GB which act as potent dislocation sources for increasing the local dislocation density. *In situ* tensile tests on the same system, however, suggest a different mechanism, where sulphur segregation at GBs is speculated to prevent dislocation transmission, ultimately resulting in intergranular fracture [63]. While the above explanation aligns well with the experimental observations reported here, Ag segregation does not however completely restrict dislocation transmission in Cu. Furthermore, Wyrzykowski *et al.* studied the effect of temperature (77–423 K) on k in polycrystalline Al [64]. Interestingly, the specimens with a higher fraction of special GBs demonstrated higher k values. This was explained based on the differences in the distribution of GB diffusivity coefficients. For specimens with lower fraction of special GBs, higher GB diffusivity coefficients promote relaxation processes at GBs, thus resulting in more "transparent" GBs. In the present context, the variation of k with temperature could be better explained by considering indirect transmission, which is sensitive to non-conservative dislocation motion within the GB, and thus to GB diffusivity and testing temperatures (also strain rates).

Finally, taking factor (v) into consideration, GBs can influence plastic deformation by acting as sources and sinks for dislocations [10]. Verifying such processes experimentally poses an extremely challenging task and the atomic details of these processes are still largely unsolved. In this light, Borovikov *et al.* simulated the effect of Ag-segregation on dislocation nucleation from a Σ11 GB in Cu where a dramatic increase in yield stress was observed, associated with deformation mechanisms controlled by dislocation emission from the GB [65]. It is also important to consider the amount of segregation, as a higher solute concentration may negatively impact emission stress [57,66]. However, in the present case, the initial local dislocation density up to $(9.5 \pm 2.0) \times 10^{12}$ m^{-2} corresponds to a minimum dislocation spacing of ~320 nm. As a result, already existing dislocations and their multiplication could potentially mask the effect of GB dislocation sources. Hence, the impact of Ag segregation on dislocation emission by the GB could not be assessed. Nevertheless, the results clearly reveal that dislocation transmission is governed by both geometry of the adjacent slip systems and GB chemistry.

Our findings suggest that interaction of segregated solute atoms and dislocations at GBs can be an important micro-mechanism influencing plasticity in nanocrystalline alloys. Most previous computational and experimental work has focused on the segregation-induced strengthening response of nanocrystalline alloys based of GB stabilisation or GB pinning, encompassing only GB mediated deformation processes (such as GB sliding, GB dislocation sources and GB migration) [36,67,68]. GB stabilisation positively scales with the size of the segregated elements (lattice mismatch) as does the dislocation pinning capability of solutes [32,39,57]. However, the influence of segregating elements on slip transmission has largely been overlooked in experiments, while only a limited number of simulations have described its influence [30,69]. Nevertheless, producing alloys with superior properties requires a thorough understanding of the atomistic mechanisms influencing plastic deformation. It is therefore essential for both experimental and modelling studies to consider variability of segregation and its influence on slip transmission.

5. Conclusions

Using a Cu-Ag model system coupled with *in situ* micropillar compression, the effect of Ag impurity segregation at an asymmetric Σ5 GB on mechanical behaviour was successfully examined. The effect of GB segregation on the mechanical response with a specific focus on the role of local chemistry on dislocation transmission was quantitatively measured. Small pillar dimensions of ~1 μm diameter ensured that dislocation-GB interactions dominated the deformation process, even during a crystallographic alignment for multiple slip system activation. Ag enrichment at the GB leads to a significant increase in yield strength, with Bxx micropillars containing pristine Σ5 having a yield strength of 288 ± 18 MPa, compared to 318 ± 17 MPa for Bxx(Ag) micropillars containing an Ag-segregated Σ5 GB. Possible influences by solid solution strengthening, changes in misorientation or possible GB dislocation networks were ruled out by the experiments, which led to the conclusion that GB segregation of Ag enhances the transmission stress. Simulations are required to understand the exact atomistic mechanisms and resolve the physical nature of the stress increase. Thus, not only grain size refinement by GB segregation, but also the GB chemistry is an important lever to improve the strength of materials, while *in situ* micropillar compression in conjunction with local chemical analysis allows the rational study of such effects.

Declaration of Competing Interest

The authors declare that they have no known competing financial interests or personal relationships that could have appeared to influence the work reported in this paper.

Acknowledgments

The authors gratefully thank Simon Evertz from MPIE for Ag sputtering, Christian Broß for sample surface preparation, Daniel Kurz for wet chemical analysis and Simon Rekort for assistance with conventional TEM preparation. Leon Christiansen is gratefully acknowledged for his assistance throughout the micropillar fabrication and compression experiments. The funding and support by the European Research Council (ERC) under the EU's Horizon 2020 Research and Innovation Program is gratefully acknowledged by MKB and GD (ERC Advanced Grant, GB-Correlate, Grant No. 787446).

Supplementary materials

Supplementary material associated with this article can be found, in the online version, at doi:10.1016/j.actamat.2023.119081.

References

[1] H. Bishara, S. Lee, T. Brink, M. Ghidelli, G. Dehm, Understanding grain boundary electrical resistivity in Cu: the effect of boundary structure, ACS Nano 15 (2021) 16607–16615, https://doi.org/10.1021/acsnano.1c06367.
[2] P.R. Cantwell, T. Frolov, T.J. Rupert, A.R. Krause, C.J. Marvel, G.S. Rohrer, J. M. Rickman, M.P. Harmer, Grain boundary complexion transitions, Annu. Rev. Mater. Res. 50 (2020) 465–492, https://doi.org/10.1146/annurev-matsci-081619.
[3] G. Dehm, J. Cairney, Implication of grain-boundary structure and chemistry on plasticity and failure, MRS Bull. (2022), https://doi.org/10.1557/s43577-022-00378-3.
[4] E.O. Hall, The deformation and ageing of mild steel: III Discussion of results, Proc. Phys. Soc. London. (1951) 747.
[5] J. N.Petch, The plastic deformation of polycrystalline aggregates, Iron Steel Inst 174 (1953) 25–28.
[6] J.P. Hirth, The influence of grain boundaries on mechanical properties, Metall. Trans. 3 (1972) 3047–3067.
[7] J.D. Livingston, B. Chalmers, Multiple slip in bicrystal deformation, Acta Metall. 5 (1957) 322–327.
[8] M.A. Tschopp, D.L. McDowell, Grain boundary dislocation sources in nanocrystalline copper, Scr. Mater. 58 (2008) 299–302, https://doi.org/10.1016/j.scriptamat.2007.10.010.
[9] H. Pan, Y. He, X. Zhang, Interactions between dislocations and boundaries during deformation, Materials 14 (2021) 1–48, https://doi.org/10.3390/ma14041012.
[10] J. Kacher, B.P. Eftink, B. Cui, I.M. Robertson, Dislocation interactions with grain boundaries, Curr. Opin. Solid State Mater. Sci. 18 (2014) 227–243, https://doi.org/10.1016/j.cossms.2014.05.004.

[11] T.R. Bieler, P. Eisenlohr, C. Zhang, H.J. Phukan, M.A. Crimp, Grain boundaries and interfaces in slip transfer, Curr. Opin. Solid State Mater. Sci. 18 (2014) 212–226, https://doi.org/10.1016/j.cossms.2014.05.003.

[12] J. Luster, M.A. Morris, Compatibility of dependence on deformation in two-phase Ti-AI alloys: microstructure and orientation relationships, Metall. Mater. Trans. A 26A (1995) 1745–1756.

[13] J.S. Weaver, N. Li, N.A. Mara, D.R. Jones, H. Cho, C.A. Bronkhorst, S.J. Fensin, G. T. Gray, Slip transmission of high angle grain boundaries in body-centered cubic metals: micropillar compression of pure Ta single and bi-crystals, Acta Mater. 156 (2018) 356–368, https://doi.org/10.1016/j.actamat.2018.06.046.

[14] M.D. Sangid, T. Ezaz, H. Sehitoglu, I.M. Robertson, Energy of slip transmission and nucleation at grain boundaries, Acta Mater. 59 (2011) 283–296, https://doi.org/10.1016/j.actamat.2010.09.032.

[15] J. Wang, Atomistic simulations of dislocation pileup: grain boundaries interaction, JOM 67 (2015) 1515–1525, https://doi.org/10.1007/s11837-015-1454-0.

[16] P.J. Imrich, C. Kirchlechner, C. Motz, G. Dehm, Differences in deformation behavior of bicrystalline Cu micropillars containing a twin boundary or a large-angle grain boundary, Acta Mater. 73 (2014) 240–250, https://doi.org/10.1016/j.actamat.2014.04.022.

[17] N. Kheradmand, H. Vehoff, A. Barnoush, An insight into the role of the grain boundary in plastic deformation by means of a bicrystalline pillar compression test and atomistic simulation, Acta Mater. 61 (2013) 7454–7465, https://doi.org/10.1016/j.actamat.2013.08.056.

[18] M. Heller, J.S.K.L. Gibson, R. Pei, S. Korte-Kerzel, Deformation of μm- and mm-sized Fe2.4wt%Si single- and bi-crystals with a high angle grain boundary at room temperature, Acta Mater. 194 (2020) 452–463, https://doi.org/10.1016/j.actamat.2020.04.011.

[19] K.S. Ng, A.H.W. Ngan, Deformation of micron-sized aluminium bi-crystal pillars, Philos. Mag. 89 (2009) 3013–3026, https://doi.org/10.1080/14786430903164614.

[20] R. Hosseinabadi, H. Riesch-Oppermann, J.P. Best, G. Dehm, C. Kirchlechner, Size scaling in bi-crystalline Cu micropillars containing a coherent twin boundary, Acta Mater. 230 (2022), https://doi.org/10.1016/j.actamat.2022.117841.

[21] A. Kunz, S. Pathak, J.R. Greer, Size effects in Al nanopillars: single crystalline vs. bicrystalline, Acta Mater. 59 (2011) 4416–4424, https://doi.org/10.1016/j.actamat.2011.03.065.

[22] N.V. Malyar, J.S. Micha, G. Dehm, C. Kirchlechner, Size effect in bi-crystalline micropillars with a penetrable high angle grain boundary, Acta Mater. 129 (2017) 312–320, https://doi.org/10.1016/j.actamat.2017.03.003.

[23] T.B. Britton, D. Randman, A.J. Wilkinson, Nanoindentation study of slip transfer phenomenon at grain boundaries, J. Mater. Res. 24 (2009) 607–615, https://doi.org/10.1557/jmr.2009.0088.

[24] K. Endoh, S. Ii, Y. Kimura, T. Sasaki, S. Goto, T. Yokota, T. Ohmura, Effects of grain boundary geometry and boron addition on the local mechanical behavior of interstitial-free (IF) steels, Mater. Trans. 62 (2021) 1479–1488, https://doi.org/10.2320/matertrans.MT-M2021128.

[25] X. Maeder, W.M. Mook, C. Niederberger, J. Michler, Quantitative stress/strain mapping during micropillar compression, Philos. Mag. 91 (2011) 1097–1107, https://doi.org/10.1080/14786435.2010.505178.

[26] M.D. Uchic, D.M. Dimiduk, J.N. Florando, W.D. Nix, Sample dimensions influence strength and crystal plasticity, Science 305 (2004) 986–989, https://doi.org/10.1126/science.1098993.

[27] N. Kheradmand, H. Vehoff, Orientation gradients at boundaries in micron-sized bicrystals, Adv. Eng. Mater. 14 (2012) 153–161, https://doi.org/10.1002/adem.201100242.

[28] N. Li, J. Wang, X. Zhang, A. Misra, In-situ TEM study of dislocation-twin boundaries interaction in nanotwinned Cu films, JOM 63 (2011) 62–73.

[29] G. Dehm, B.N. Jaya, R. Raghavan, C. Kirchlechner, Overview on micro- and nanomechanical testing: new insights in interface plasticity and fracture at small length scales, Acta Mater. 142 (2018) 248–282, https://doi.org/10.1016/j.actamat.2017.06.019.

[30] I. Adlakha, K.N. Solanki, Critical assessment of hydrogen effects on the slip transmission across grain boundaries in α-Fe, Proc. R. Soc. A: Math., Phys. Eng. Sci. 472 (2016), https://doi.org/10.1098/rspa.2015.0617.

[31] Z. Huang, F. Chen, Q. Shen, L. Zhang, T.J. Rupert, Combined effects of non-metallic impurities and planned metallic dopants on grain boundary energy and strength, Acta Mater. 166 (2019) 113–125, https://doi.org/10.1016/j.actamat.2018.12.031.

[32] N.Q. Vo, J. Schäfer, R.S. Averback, K. Albe, Y. Ashkenazy, P. Bellon, Reaching theoretical strengths in nanocrystalline Cu by grain boundary doping, Scr. Mater. 65 (2011) 660–663, https://doi.org/10.1016/j.scriptamat.2011.06.048.

[33] S. Özerinç, K. Tai, N.Q. Vo, P. Bellon, R.S. Averback, W.P. King, Grain boundary doping strengthens nanocrystalline copper alloys, Scr. Mater. 67 (2012) 720–723, https://doi.org/10.1016/j.scriptamat.2012.06.031.

[34] N.V. Malyar, G. Dehm, C. Kirchlechner, Strain rate dependence of the slip transfer through a penetrable high angle grain boundary in copper, Scr. Mater. 138 (2017) 88–91, https://doi.org/10.1016/j.scriptamat.2017.05.042.

[35] A. Gupta, J. Gruber, S.S. Rajaram, G.B. Thompson, D.L. McDowell, G.J. Tucker, On the mechanistic origins of maximum strength in nanocrystalline metals, npj Comput. Mater. 6 (2020), https://doi.org/10.1038/s41524-020-00425-0.

[36] D.E. Spearot, G.J. Tucker, A. Gupta, G.B. Thompson, Perspective: mechanical properties of stabilized nanocrystalline FCC metals, J. Appl. Phys. 126 (2019), https://doi.org/10.1063/1.5114706.

[37] D. Raabe, M. Herbig, S. Sandlöbes, Y. Li, D. Tytko, M. Kuzmina, D. Ponge, P. P. Choi, Grain boundary segregation engineering in metallic alloys: a pathway to the design of interfaces, Curr. Opin. Solid State Mater. Sci. 18 (2014) 253–261, https://doi.org/10.1016/j.cossms.2014.06.002.

[38] N.A. Enikeev, I.V. Lomakin, M.M. Abramova, A.M. Mavlyutov, A.A. Lukyanchuk, A.S. Shutov, X. Sauvage, Plasticity of an extra-strong nanocrystalline stainless steel controlled by the "dislocation-segregation" interaction, Mater. Lett. 301 (2021), https://doi.org/10.1016/j.matlet.2021.130235.

[39] Z. Huang, P. Wang, F. Chen, Q. Shen, L. Zhang, Understanding solute effect on grain boundary strength based on atomic size and electronic interaction, Sci. Rep. 10 (2020), https://doi.org/10.1038/s41598-020-74065-1.

[40] C.M. Barr, S.M. Foiles, M. Alkayyali, Y. Mahmood, P.M. Price, D.P. Adams, B. L. Boyce, F. Abdeljawad, K. Hattar, The role of grain boundary character in solute segregation and thermal stability of nanocrystalline Pt-Au, Nanoscale 13 (2021) 3552–3563, https://doi.org/10.1039/d0nr07180c.

[41] M. Herbig, D. Raabe, Y.J. Li, P. Choi, S. Zaefferer, S. Goto, Atomic-scale quantification of grain boundary segregation in nanocrystalline material, Phys. Rev. Lett. 112 (2013), https://doi.org/10.1103/PhysRevLett.112.126103.

[42] T. Frolov, K.A. Darling, L.J. Kecskes, Y. Mishin, Stabilization and strengthening of nanocrystalline copper by alloying with tantalum, Acta Mater. 60 (2012) 2158–2168, https://doi.org/10.1016/j.actamat.2012.01.011.

[43] P.R. Subramanian, J.H. Perepezko, The Ag-Cu (silver-copper) system, J. Phase Equilib. 14 (1993) 62–75.

[44] N.J. Peter, M.J. Duarte, C. Kirchlechner, C.H. Liebscher, G. Dehm, Faceting diagram for Ag segregation induced nanofaceting at an asymmetric Cu tilt grain boundary, Acta Mater. 214 (2021), https://doi.org/10.1016/j.actamat.2021.116960.

[45] I. Blum, S.-I. Baik, M.G. Kanatzidis, D.N. Seidman, An integral method for the calculation of the reduction in interfacial free energy due to interfacial segregation, doi:10.48550/arXiv.2003.01246.

[46] P.J. Imrich, C. Kirchlechner, G. Dehm, Influence of inclined twin boundaries on the deformation behavior of Cu micropillars, Mater. Sci. Eng. A 642 (2015) 65–70, https://doi.org/10.1016/j.msea.2015.06.064.

[47] I. Tiba, T. Richeton, C. Motz, H. Vehoff, S. Berbenni, Incompatibility stresses at grain boundaries in Ni bicrystalline micropillars analyzed by an anisotropic model and slip activity, Acta Mater. 83 (2015) 227–238, https://doi.org/10.1016/j.actamat.2014.09.033.

[48] S. Korte, W.J. Clegg, Discussion of the dependence of the effect of size on the yield stress in hard materials studied by microcompression of MgO, Philos. Mag. 91 (2011) 1150–1162, https://doi.org/10.1080/14786435.2010.505179.

[49] D. Mercier, C. Zambaldi, T.R. Bieler, A Matlab toolbox to analyze slip transfer through grain boundaries, in: IOP Conference Series Materials Science Engineering, Institute of Physics Publishing, 2015, https://doi.org/10.1088/1757-899X/82/1/012090.

[50] O. Kraft, P.A. Gruber, R. Mönig, D. Weygand, Plasticity in confined dimensions, Annu. Rev. Mater. Res. 40 (2010) 293–317, https://doi.org/10.1146/annurev-matsci-082908-145409.

[51] X. Zhang, S. Lu, B. Zhang, X. Tian, Q. Kan, G. Kang, Dislocation–grain boundary interaction-based discrete dislocation dynamics modeling and its application to bicrystals with different misorientations, Acta Mater. 202 (2021) 88–98, https://doi.org/10.1016/j.actamat.2020.10.052.

[52] I.C. Lim, R. Raj, Continuity of slip screw and mixed crystal dislocations across bicrystals of Nickel at 573K, Acta Metall. 33 (1985) 1577–1583.

[53] J.A. Venables, The nucleation and propagation of deformation twins, J. Phys. Chem. Solids Pergamon Press. 25 (1964) 693–700.

[54] C.J. Wang, B.N. Yao, Z.R. Liu, X.F. Kong, D. Legut, R.F. Zhang, Y. Deng, Effects of solutes on dislocation nucleation and interface sliding of bimetal semi-coherent interface, Int. J. Plast. 131 (2020), https://doi.org/10.1016/j.ijplas.2020.102725.

[55] R.L. Fleischer, Substitutional solution hardening, Acta Metall. 11 (1963) 203–209.

[56] Y. Cheng, M. Mrovec, P. Gumbsch, Atomistic simulations of interactions between the 1/2⟨111⟩edge dislocation and symmetric tilt grain boundaries in tungsten, Philos. Mag. 88 (2008) 547–560, https://doi.org/10.1080/14786430801894577.

[57] V. Turlo, T.J. Rupert, Grain boundary complexions and the strength of nanocrystalline metals: dislocation emission and propagation, Acta Mater. 151 (2018) 100–111, https://doi.org/10.1016/j.actamat.2018.03.055.

[58] N.J. Peter, PhD thesis, Ruhr-Universität Bochum, 2021, https://doi.org/10.13154/294-8312.

[59] S. Chu, P. Liu, Y. Zhang, X. Wang, S. Song, T. Zhu, Z. Zhang, X. Han, B. Sun, M. Chen, In situ atomic-scale observation of dislocation climb and grain boundary evolution in nanostructured metal, Nat. Commun. 13 (2022), https://doi.org/10.1038/s41467-022-31800-8.

[60] C.M. Lousada, P.A. Korzhavyi, Single vacancies at Σ5, Σ9 and Σ11 grain boundaries of copper and the geometrical factors that affect their site preference, J. Phys. Chem. Solids 169 (2022), https://doi.org/10.1016/j.jpcs.2022.110833.

[61] Z.C. Cordero, B.E. Knight, C.A. Schuh, Six decades of the Hall–Petch effect – a survey of grain-size strengthening studies on pure metals, Int. Mater. Rev. 61 (2016) 495–512, https://doi.org/10.1080/09506608.2016.1191808.

[62] S. Floreen, J.H. Westbrooks, Grain boundary segregation and the grain size dependence of strength of nickel-sulfur alloys, Acta Metall. 17 (1969) 1175–1181.

[63] T.C. Lee, I.M. Robertson, H.K. Birnbaum, An HVEM in situ deformation study of Nickel doped with Sulfur, Acta Metall. 37 (1989) 407–415.

[64] J.W. Wyrzykowski, M.W. Grabski, The Hall–Petch relation in aluminium and its dependence on the grain boundary structure, Phil. Mag. A 53 (1986) 505–520, https://doi.org/10.1080/01418618608242849.

[65] V. Borovikov, M.I. Mendelev, A.H. King, Effects of solutes on dislocation nucleation from grain boundaries, Int. J. Plast. 90 (2017) 146–155, https://doi.org/10.1016/j.ijplas.2016.12.009.

[66] V. Borovikov, M.I. Mendelev, A.H. King, Solute effects on interfacial dislocation emission in nanomaterials: nucleation site competition and neutralization, Scr. Mater. 154 (2018) 12–15, https://doi.org/10.1016/j.scriptamat.2018.05.011.

[67] J. Hu, Y.N. Shi, X. Sauvage, G. Sha, K. Lu, Grain boundary stability governs hardening and softening in extremely fine nanograined metals, Science 355 (2017) 1292–1296, https://doi.org/10.1126/science.aal5166, 1979.
[68] V. Yamakov, D. Wolf, S.R. Phillpot, A.K. Mukherjee, H. Gleiter, Deformation-mechanism map for nanocrystalline metals by molecular-dynamics simulation, Nat. Mater. 3 (2004) 43–47, https://doi.org/10.1038/nmat1035.
[69] F. Shuang, K.E. Aifantis, Using molecular dynamics to determine mechanical grain boundary energies and capture their dependence on residual Burgers vector, segregation and grain size, Acta Mater. 195 (2020) 358–370, https://doi.org/10.1016/j.actamat.2020.05.014.